Received: 2 July 2020 | Revised: 14 November 2020 | Accepted: 27 December 2020 | Published on: 19 January 2021

DOI: 10.1002/joc.6997

RESEARCH ARTICLE

International Journal of Climatology RMetS

The summer precipitation response of latewood tree-ring chronologies in the southwestern United States

Ian M. Howard[1] | **David W. Stahle**[1] | **Max C. A. Torbenson**[2] | **Daniel Griffin**[3]

[1]Department of Geosciences, University of Arkansas, Fayetteville, Arkansas

[2]Department of Civil, Environmental and Geodetic Engineering, The Ohio State University, Columbus, Ohio

[3]Department of Geography, Environment and Society, University of Minnesota, Minneapolis, Minnesota

Correspondence
Ian M. Howard, Department of Geosciences, University of Arkansas, Fayetteville, AR 72701.
Email: ihowardksu@gmail.com

Funding information
National Science Foundation, Grant/Award Numbers: AGS-1266014, AGS-1702894

Abstract

Latewood width tree-ring chronologies from arid-site conifers in the southwestern United States are correlated with precipitation during portions of the summer monsoon season. The onset date and length of the monsoon season varies across the region, and these regional differences in summer rainfall climatology may impact the strength and timing of the warm season precipitation response of latewood chronologies. The optimal latewood response to summer precipitation is computed on a daily basis using 67 adjusted latewood chronologies (LWa) from the southwestern United States, adjusted to remove correlation with preceding earlywood growth. Most LWa chronologies are significantly correlated with precipitation summed over a period of approximately 4 weeks (29 days) in early summer. This early summer precipitation signal is present in most ponderosa pine chronologies across the study area. It is also evident in Douglas-fir chronologies, but only from southern Arizona and New Mexico. The Julian date of summer precipitation onset increases from south to north in the instrumental precipitation data for the southwestern United States. The timing of the early summer season precipitation response in most LWa chronologies also tends to occur later in the summer from southeastern Arizona into northern New Mexico and eastern Colorado. Principal components analysis of the LWa chronologies reproduces two of the three most important spatial modes of early summer precipitation covariability seen in the instrumental data. The first PC of LWa is related to the same atmospheric circulation features associated with PC1 of instrumental early summer precipitation, including cyclonic circulation over the southwestern United States and moisture advection from the eastern Pacific. Correlation analyses between antecedent cool season precipitation and early summer rainfall using instrumental and tree-ring reconstructed precipitation indicates that the tree-ring data reproduce the multi-decadal variability in correlation between seasons seen in the instrumental data.

KEYWORDS

latewood width, optimal daily precipitation response, *Pinus ponderosa*, *Pseudotsuga menziesii*, summer wet season onset, withdrawal, duration, tree-ring chronologies

1 | INTRODUCTION

Warm season precipitation associated with the North American Monsoon System (NAMS) is a vital water resource to the montane ecosystems of northern Mexico and the southwestern United States (Adams and Comrie, 1997). The contribution of summer monsoon precipitation is highest over the Sierra Madre Occidental in northern Mexico extending northward into southern Arizona and New Mexico (Douglas *et al*., 1993), but the influence of the monsoon circulation may encompass much of the western North American plateau even though the contribution to annual totals is lower (Hales, 1972; Reiter and Tang, 1984; Tang and Reiter, 1984). There is some evidence that the timing of when summer rains arrive has changed in recent decades as indicated by delays in the onset, peak, and demise of the monsoon across the southwestern United States (Grantz et al., 2007). Though there is high uncertainty, global circulation models suggest that early season monsoon precipitation in June and July is projected to decline, but late summer totals in September are projected to increase (Cook and Seager, 2013). Combined with higher summer temperatures and increased evaporative demand (Williams *et al*., 2013), decreases in early summer precipitation will potentially increase agricultural and forest stress during the summer growing season (McDowell *et al*., 2016). Changes in the arrival and intensity of monsoon rains can have a significant impact on dryland agriculture and ranching, wildfire activity, and plant survival and productivity (Germaine and McPherson, 1998; Swetnam and Betancourt, 1998; Ray *et al*., 2007). However, the possible future impacts of changing summer precipitation seasonality on forest ecosystems of the southwestern United States will likely vary because the importance of summer moisture to plant growth varies across the region (Ray *et al*., 2007; Szejner *et al*., 2016). As an example, growth and productivity of conifers located near the border of the southwestern United States and Mexico are tightly coupled to monsoon rains, but at the northern boundary of the NAMS in southern Utah and Colorado the biophysical processes associated with tree growth are more heavily influenced by winter and spring moisture (Szejner *et al*., 2016).

Tree-ring chronologies of annual ring width (RW) from the southwestern United States are not ideal for reconstructing summer climate because total RW tends to be correlated with climate conditions that influence the availability of soil moisture across several months prior to and during the growing season (Douglass, 1920; Fritts, 1976). In recent years, sub-annual tree-ring chronologies of earlywood (EW) and latewood (LW) width from Mexico and the southwestern United States have made it possible to produce discrete estimates of precipitation during the cool and monsoon seasons (e.g., Cleaveland, 1986; Cleaveland *et al*., 2003; Villanueva-Diaz *et al*., 2007; Stahle *et al*., 2009; Faulstich *et al*., 2013; Griffin *et al*., 2013; Woodhouse *et al*., 2013; Stahle *et al*., 2020). LW width chronologies are often very highly correlated with EW chronologies (Torbenson *et al*., 2016) due to significant sharing of carbohydrate resources and soil moisture pools (Szejner *et al*., 2018) and tend to be impacted by climate variables that also influence EW width, sometimes including a partial response to summer rainfall. Adjusted latewood chronologies (LWa) are the residuals from a regression of LW on EW width chronologies and are therefore independent of the variability in the EW chronologies (Meko and Baisan, 2001; Stahle *et al*., 2009; Griffin *et al*., 2011; Griffin, 2013). Adjusted latewood chronologies from the southwestern United States tend to be best correlated with precipitation in July and August associated with the NAMS (Meko and Baisan, 2001; Therrell *et al*., 2002; Stahle *et al*., 2009; Faulstich *et al*., 2013; Griffin, 2013; Griffin *et al*., 2013; Woodhouse *et al*., 2013). Distinct seasonal climate signals in LW and LWa growth chronologies have also been identified in conifer chronologies from western Canada (Watson and Luckman, 2002), the interior Rocky Mountains (Crawford *et al*., 2015), western Washington (Dannenberg and Wise, 2016), the south-central United States (Torbenson and Stahle, 2018), the western Great Plains (Howard *et al*., 2019), as well for many other tree species worldwide (e.g., Lebourgeois *et al*., 2005).

In dendroclimatology, climate-response analyses often use instrumental climate variables calculated on monthly, seasonal, or annual timescales. However, the tree growth response to environmental conditions may not be best represented with analyses based on monthly or seasonal data. Previous studies have utilized daily observations to investigate the optimal periods of moisture or temperature response in tree-ring data (e.g., Deslauriers *et al*., 2003; Beck *et al*., 2013; Land *et al*., 2017; Jevšenak, 2019; Howard and Stahle, 2020) and in simulated tree-ring chronologies (Anchukaitis *et al*., 2006). Higher correlations with climate can sometimes be found using variables not restricted to monthly or seasonal averages. The use of daily data can also reveal low-frequency changes in the timing of the tree growth response to climate during the growing season (Anchukaitis *et al*., 2006; Beck *et al*., 2013; Jevšenak, 2019). The currently published reconstructions of summer precipitation in the southwestern United States were targeted at monthly and seasonal rainfall totals for a single site or region and did not explore the relationship between summer precipitation and tree growth at the daily timescales fundamental to monsoon variability, dynamics, and ecosystem interactions. The identification of summer moisture

proxies across the southwestern United States is important for analyses of the climate dynamics responsible for monsoon precipitation variability and its impact on ecosystem productivity, for the detection of possible long-term changes to summer precipitation due to anthropogenic forcing, and for investigations of the potential link between cool season climate conditions and the onset and intensity of summer rains (e.g., Gutzler, 2000; Ellis and Hawkins, 2001; Lo and Clark, 2002). Climate response analysis using daily precipitation data may also be useful in the southwestern United States where the onset and importance of summer rains varies across the domain (Higgins *et al*., 1997; Ellis *et al*., 2004).

This article addresses the optimal precipitation response question and the dynamics of summer precipitation variability with a systematic analysis of daily instrumental data and 67 LWa chronologies of Douglas-fir (*Pseudotsuga menziesii*) and ponderosa pine (*Pinus ponderosa*), the two species most commonly used for reconstructing hydroclimate in the southwestern United States. The objectives of this study were to:

1. Map the average Julian date of onset for the summer wet season across the southwestern United States using gridded instrumental daily precipitation data.
2. Investigate the daily precipitation response of LWa chronologies in the southwestern United States and identify the onset and withdrawal dates, peak correlation, and duration of the optimal warm season precipitation signals in these sub-annual RW data.
3. Investigate the prominent spatial modes of LW growth variability for sites significantly correlated with summer precipitation to determine whether these tree-ring chronologies reproduce the major spatiotemporal modes of early summer precipitation variability over the southwestern United States.
4. Explore the climate dynamics of early summer precipitation using both instrumental and proxy tree-ring data.

2 | STUDY REGION AND THE SUMMER RAINFALL CLIMATOLOGY OF THE SOUTHWESTERN UNITED STATES

The 67 tree-ring sample sites are located across a diverse geographic range of the southwestern United States (Figure 1; Table 1) where rainfall associated with the NAMS from late June through early September contributes a substantial fraction of annual precipitation totals (Figure 2). The onset of the summer rainy season generally occurs in late June and early July in far west Texas and southern New Mexico, during the first 2 weeks of July over southern Arizona, and gradually becomes later with an increase in latitude (see Figure 4; Higgins *et al*., 1997; Ellis *et al*., 2004; Liebmann *et al*., 2008). Summer monsoon moisture in July and August contributes the highest percentage of the total annual precipitation for the areas of southeastern Arizona and western New Mexico (Figure 2b,c), with a pronounced peak in daily rainfall totals in July and remaining elevated through September (Figure 3c). In north-central Arizona, the precipitation climatology is bimodal with high contributions

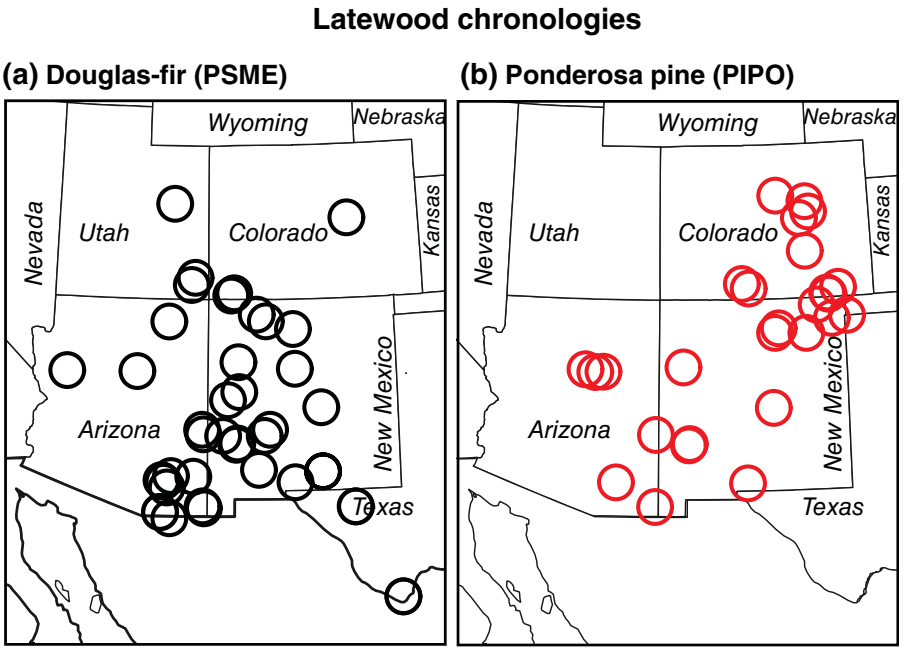

FIGURE 1 Site maps illustrating the geographic distribution of the (a) Douglas-fir and (b) ponderosa pine LWa chronologies used in this analysis. A total of 40 Douglas-fir and 27 ponderosa pine chronologies were used. Note there are several locations where multiple chronologies are present [Colour figure can be viewed at wileyonlinelibrary.com]

TABLE 1 The name, location, species, and summer precipitation response of 67 adjusted LW width chronologies from the southwest are tabulated

Site name	Summer	Lat	Lon	Species	Onset	Withdrawal	Duration	Peak *r*	O-30	W-30	*r*-30
Arizona											
Bear Canyon	X	32.23	−110.41	PSME	172	194	22	.62	189	219	.51
Bear Canyon	X	32.23	−110.41	PIPO	183	218	35	.58	195	225	.47
Douglas Canyon	X	32.38	−110.18	PSME	188	223	35	.81	199	229	.66
Florida Low	X	31.44	−110.50	PSME	178	215	37	.67	195	225	.49
Florida Saddle	X	31.43	−110.50	PSME	179	202	23	.63	191	221	.49
Fort Valley	X	35.16	−111.45	PIPO	194	239	45	.67	215	245	.44
Ladybug Peak	X	32.37	−109.49	PSME	180	209	29	.49	197	227	.39
Onion Saddle	X	31.55	−109.16	PSME	173	232	59	.70	176	206	.66
Potato Patch		35.05	−113.54	PSME	153	228	75	.76	—	—	—
Rhyolite Canyon	X	31.60	−109.20	PSME	179	202	23	.73	184	214	.58
Rhyolite Canyon	X	31.60	−109.20	PIPO	180	218	38	.69	194	224	.52
Rincon Peak	X	32.08	−110.31	PSME	182	194	12	.64	190	220	.48
Santa Catalina	X	32.27	−110.47	PSME	188	198	10	.63	198	228	.51
Scheelite Canyon	X	31.28	−110.21	PSME	176	204	28	.54	188	218	.38
Tsegi Canyon		36.41	−110.32	PSME	157	193	36	.53	—	—	—
Wahl Knoll	X	33.60	−109.23	PSME	192	204	12	.54	199	229	.29
Walnut Canyon		35.10	−111.31	PSME	127	196	69	.70	—	—	—
Walnut Canyon	X	35.10	−111.31	PIPO	190	251	61	.74	214	244	.62
White Canyon		37.37	−109.60	PSME	158	170	12	.74	—	—	—
Winona Canyon	X	35.09	−111.31	PIPO	188	205	17	.65	191	221	.53
Colorado											
Black Forest East	X	39.50	−104.22	PIPO	193	219	26	.68	205	235	.58
Gotera Rincon	X	37.06	−103.57	PIPO	200	210	10	.65	209	239	.47
Jefferson County	X	39.68	−105.20	PIPO	197	219	22	.70	203	233	.50
Kim	X	37.23	−103.25	PIPO	190	210	20	.66	197	227	.55
Mancos River		37.16	−108.21	PSME	116	203	87	.70	—	—	—
Mesa de Maya	X	37.10	−103.62	PIPO	199	210	11	.42	208	238	.27
Mesa Verde Fir		37.10	−108.31	PSME	157	171	14	.80	—	—	—
Ridge Road	X	39.23	−104.12	PIPO	199	220	21	.48	208	238	.38
South Fork	X	37.40	−106.40	PIPO	199	226	27	.65	213	243	.56
Turkey Creek	X	38.21	−104.29	PIPO	192	218	26	.64	202	232	.51
Valley View	X	39.07	−104.43	PSME	184	195	11	.58	184	214	.40
Valley View	X	39.07	−104.43	PIPO	190	225	35	.60	183	213	.40
Vera Platt	X	37.28	−106.18	PIPO	199	211	12	.61	210	240	.44
New Mexico											
Black Mountain	X	33.21	−108.16	PSME	180	209	29	.64	190	220	.52
Black Mountain		33.21	−108.16	PIPO	234	245	11	.46	—	—	—
Black River	X	33.48	−109.19	PSME	190	204	14	.58	198	228	.43
Black River	X	33.48	−109.19	PIPO	185	209	24	.48	201	231	.37
Cornay Ranch	X	36.80	−103.98	PIPO	192	212	20	.64	204	234	.57
Ditch Canyon		36.60	−107.48	PSME	133	149	16	.60	—	—	—

TABLE 1 (Continued)

New Mexico											
Echo Amp.		36.21	−106.32	PSME	134	181	47	.61	—	—	—
El Malpais		34.58	−108.06	PSME	154	223	69	.64	—	—	—
Emory Pass	X	32.55	−107.46	PSME	174	224	50	.59	191	221	.47
Filmore Canyon	X	32.20	−106.34	PIPO	179	222	43	.63	201	231	.47
Fox Mountain		34.37	−108.42	PSME	133	151	18	.65	—	—	—
Gallinas Mtn.	X	34.15	−105.48	PSME	173	218	45	.62	194	224	.47
Gallinas Mtn.	X	34.15	−105.48	PIPO	189	220	31	.64	205	235	.44
Garcia Park		36.22	−105.24	PIPO	139	152	13	.39	—	—	—
Guadalupe Mtn.		31.54	−104.51	PSME	139	158	19	.61	—	—	—
Kenton	X	36.49	−103.01	PIPO	191	223	32	.73	202	232	.59
Luna South		33.44	−108.57	PSME	162	194	32	.58	—	—	—
Magdelena Mtn.	X	33.59	−107.10	PSME	179	222	43	.69	196	226	.53
Mill Canyon	X	36.07	−104.35	PIPO	180	226	46	.70	219	249	.60
Organ Mountain		32.21	−106.34	PSME	155	199	44	.74	—	—	—
Pueblita Canyon		36.42	−107.19	PSME	158	175	17	.71	—	—	—
Rio Pueblo	X	36.10	−105.36	PIPO	202	225	23	.69	217	247	.58
Sandia	X	35.17	−106.28	PSME	167	229	62	.76	199	229	.57
Satan Pass		35.36	−108.08	PSME	127	170	43	.60	—	—	—
Sierra Grande	X	36.43	−103.51	PIPO	195	208	13	.57	202	232	.42
Smith Mountain		33.43	−107.27	PSME	149	238	89	.49	—	—	—
Sunspot Update	X	32.48	−105.48	PSME	189	225	36	.69	208	238	.48
Sunspot	X	32.48	−105.48	PSME	183	202	19	.65	206	236	.51
Turkey Springs	X	35.24	−108.32	PIPO	197	232	35	.64	213	243	.55
Wolf Hollow	X	33.24	−108.13	PSME	178	214	36	.72	191	221	.62
Wolf Hollow		33.24	−108.13	PIPO	154	216	62	.54	—	—	—
Texas											
Big Bend	X	29.15	−103.18	PSME	194	210	16	.33	202	232	.15
Utah											
Beef Basin		37.56	−109.48	PSME	134	149	15	.59	—	—	—
Harmon Canyon		39.48	−110.2	PSME	151	197	46	.74	—	—	—

Note: The 46 chronologies with a discrete summer precipitation signal are indicated (X) in column 2 ('Summer'). The onset and withdrawal dates (W-30 and O-30, respectively), as well the peak Pearson's *r*-value (*r*-30) for the optimal moisture response using a fixed 30-day window smoothed with a 30-day running average are included for those sites with a discrete summer moisture signal (see Figure 5).

from winter moisture associated with mid-latitude storm systems, along with summer rains from the NAMS that typically impact the region beginning in early July (Figure 3a). In north-central New Mexico, summer precipitation is dominant, but the peak in daily rainfall rates is less pronounced compared to southern Arizona (Figure 3d). At the far northeastern boundary of the NAMS, daily precipitation rates are characterized by two peaks, one in late spring associated with major synoptic storm systems, and a secondary peak in midsummer that is connected to the monsoon circulation and low-level moisture advection from the Gulf of Mexico (Figure 3b; Hansen *et al*., 1978). These differences in summer precipitation climatology may be imprinted on the LW tree growth response to climate of arid-site conifers from the southwestern United States.

3 | DATA AND METHODS

3.1 | LW width chronology development

Paired EW and LW width measurements from 40 Douglas-fir and 27 ponderosa sites were used to calculate the

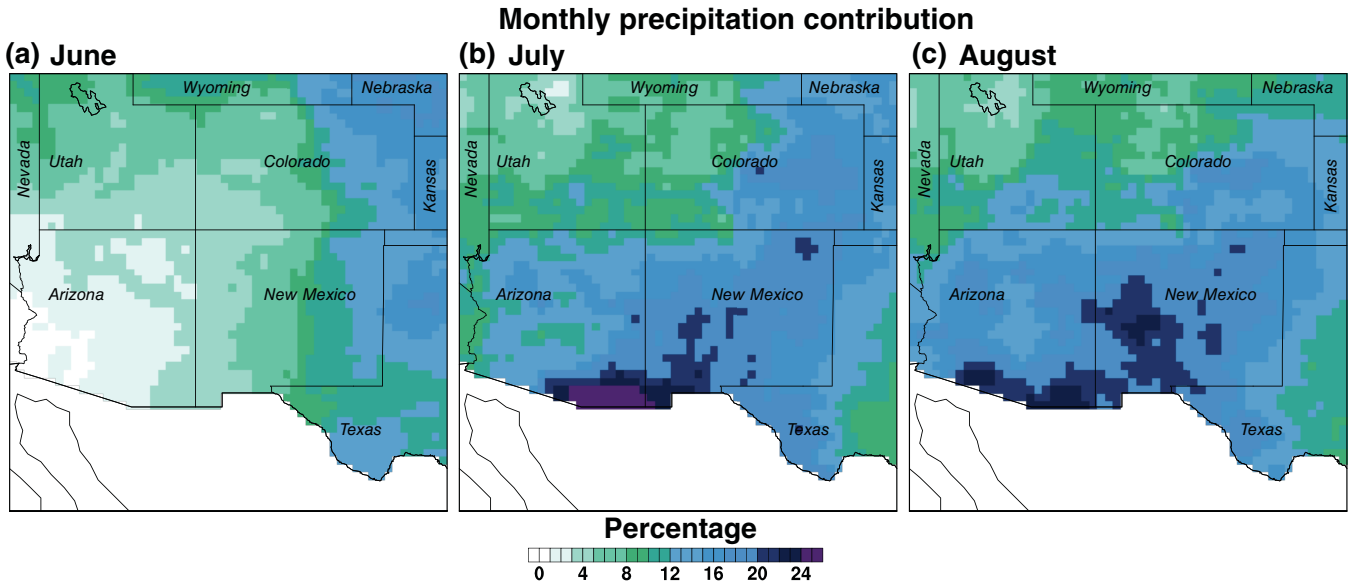

FIGURE 2 The percent contribution of monthly precipitation totals for (a) June, (b) July, and (c) August are plotted for the southwestern United States calculated for the period 1948–2019 using the gridded daily data. Note the influence of the NAMS beginning in July over much of Arizona, New Mexico, and higher precipitation contributions also extend northeastward into Colorado and the western Great Plains [Colour figure can be viewed at wileyonlinelibrary.com]

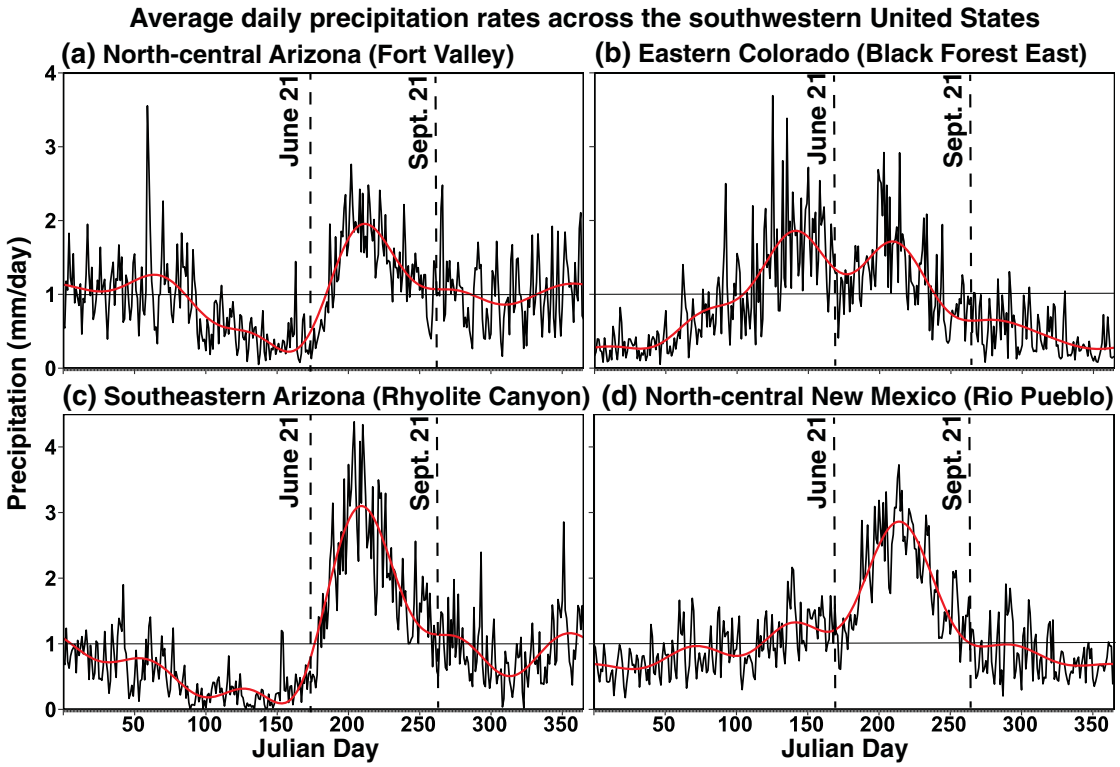

FIGURE 3 Climatological average daily precipitation rates (mm/day) are plotted for four grid points closest to LWa chronologies in different regions of the southwestern United States, including (a) north-central Arizona, (b) eastern Colorado, (c) southeastern Arizona, (d) north-Central New Mexico. These series have been smoothed with a 5-day running mean. The average daily precipitation rates are calculated for the period 1948–1991 and are similar if calculated for the full instrumental period from 1948–2019. The 1 mm threshold is also plotted (solid horizontal line). Dashed vertical lines represent the astronomical starts of summer (June 21) and fall (September 21) [Colour figure can be viewed at wileyonlinelibrary.com]

TABLE 2 Tree-ring metadata for the 67 chronologies used in this study

Site name Arizona	Elevation (m)	Chronology length	Archive collector
Bear Canyon	1,877	1698–2009	Many (Griffin)
Bear Canyon	1,877	1838–2009	Many (Griffin)
Douglas Canyon	2,074	1652–2008	Harlan & Meko (Griffin)
Florida Low	2,278	1628–2008	Graybill (Griffin)
Florida Saddle	235	1490–2008	Schulman, Graybill & Stokes (Griffin)
Fort Valley	2,260	1815–2008	Griffin
Ladybug Peak	2,667	1626–2008	Harlan (Griffin)
Onion Saddle	2,316	1608–2010	Adams (Griffin)
Potato Patch	2,300	1797–2008	Stokes (Griffin)
Rhyolite Canyon	1,828	1618–2010	Graybill (Griffin)
Rhyolite Canyon	1,828	1576–2010	Graybill (Griffin)
Rincon Peak	2,205	1591–2008	Graybill (Griffin)
Santa Catalina	2,746	1536–2009	Harlan (Griffin)
Scheelite Canyon	1,812	1630–2009	Adams (Griffin)
Tsegi Canyon	2,068	381–2008	Douglass & Dean (Griffin)
Wahl Knoll	2,969	1366–2008	Meko (Griffin)
Walnut Canyon	1,995	1645–2010	Graybill & Stokes (Griffin)
Walnut Canyon	1,995	1528–2010	Graybill & Stokes (Griffin)
White Canyon	1,895	1347–2009	Dean (Griffin)
Winona Canyon	2,172	1667–1991	Unknown
Colorado			
Black Forest East	1,809	1690–1998	Woodhouse & Brown*
Gotera Rincon	1,790	1372–1997	Woodhouse & Brown*
Jefferson County	2,241	1531–2002	Woodhouse & Lukas*
Kim	1,743	1698–1998	Woodhouse & Brown*
Mancos River	2,494	722–2011	Stahle
Mesa de Maya	1,930	1631–1997	Woodhouse & Brown*
Mesa Verde Fir	2,042	480–2008	Schulman & Cleaveland (Griffin)
Ridge Road	1,872	1779–1997	Woodhouse & Brown*
South Fork	2,591	1556–2008	Woodhouse (Griffin)
Turkey Creek	2,176	1643–2003	Woodhouse & Lukas*
Valley View	2,217	1539–1997	Woodhouse & Brown*
Valley View	2,220	1649–1998	Woodhouse & Brown*
Vera Platt	2,835	1661–2008	Woodhouse (Griffin)
New Mexico			
Black Mountain	2,489	1304–2008	Graybill, Meko & Baisan (Griffin)
Black Mountain	2,489	1838–2009	Graybill, Meko & Baisan (Griffin)
Black River	2,434	1565–2008	Graybill (Griffin)
Black River	2,434	1657–2008	Adams & Meko (Griffin)
Cornay Ranch	2,221	1613–1998	Woodhouse & Brown*
Ditch Canyon	2,036	1610–2008	Cleaveland & Dean (Griffin)
Echo Amp.	2,029	1295–2008	Dean & Touchan (Griffin)

(Continues)

TABLE 2 (Continued)

New Mexico			
El Malpais	2,205	590–2004	Grissino-Mayer
Emory Pass	2,540	1838–2009	Griffin
Filmore Canyon	2,133	1306–2008	Grissino-Mayer, Baisan & Morino (Griffin)
Fox Mountain	2,707	1591–2009	Stockton (Griffin)
Gallinas Mtn.	2,439	1616–2008	Stockton (Griffin)
Gallinas Mtn.	2,439	1655–2008	Stockton (Griffin)
Garcia Park	2,718	1879–2008	Swetnam (Griffin)
Guadalupe Mtn.	2,417	1537–1991	Stahle
Kenton	1,693	1635–2014	Howard & Stahle
Luna South	2,600	1738–2009	Stockton (Griffin)
Magdelena Mtn.	3,044	622–2008	Grissino-Mayer, Baisan & Morino (Griffin)
Mill Canyon	1,745	1584–2015	Woodhouse & Brown*
Organ Mountain	2,475	1597–2009	Stokes (Griffin)
Pueblita Canyon	2,005	1643–2009	Cleaveland & Dean (Griffin)
Rio Pueblo	2,455	1541–2008	Swetnam (Griffin)
Sandia	2,204	925–1995	Baisan
Satan Pass	2,306	1313–2008	Dean (Griffin)
Sierra Grande	2,447	1624–2014	Howard & Stahle
Smith Mountain	2,011	816–2008	Griffin
Sunspot Update	2,870	1627–2008	Stahle
Sunspot	2,870	1628–1991	Griffin
Turkey Springs	2,374	1595–2008	Dean (Griffin)
Wolf Hollow	2,532	1669–2008	Griffin
Wolf Hollow	2,532	1597–2008	Griffin
Texas			
Big Bend	954	1493–1991	Cook
Utah			
Beef Basin	2,181	351–2005	Meko
Harmon Canyon	2,134	0–2007	Meko

Note: The original archive collectors are provided, and if (Griffin) is listed that indicates these sites were updated by Griffin *et al*. (2013). The symbol * indicates these collections were remeasured for earlywood and latewood width by Howard *et al*. (2019) and Howard and Stahle (2020).

LWa chronologies (Figure 1; Table 1). The majority of these sites were originally collected by previous investigators (Woodhouse and Brown, 2001; Stahle *et al*., 2009), but a number of sites have either been updated or re-measured for EW and LW width (Table 2; Griffin, 2013; Howard *et al*., 2019). New chronologies of ponderosa pine EW and LW width have been developed at sites in northeastern New Mexico (Table 2; Howard *et al*., 2019). The measured ring-width series of EW and LW were detrended using a cubic smoothing spline with a 0.50 frequency response at a wavelength equal to 70% of each measured series. The growth indices were averaged into the respective EW and LW index chronology using the robust mean-value function (Cook, 1985). The autocorrelation present in each chronology was removed using autoregressive modelling (Meko, 1981) to produce the residual chronologies. Though EW and LW width chronologies tend to retain separate seasonal climate information and have been used to separately reconstruct cool or warm season precipitation (e.g., Cleaveland *et al*., 2003; Torbenson and Stahle, 2018; Stahle *et al*., 2020), the correlation between EW and LW at a given site can be so high that the strong winter–spring signal in EW width obscures any separate summertime signal that might also be recorded in LW width (Torbenson *et al*., 2016). This autocorrelation between EW and LW can be removed using regression techniques.

Meko and Baisan (2001) regressed the LW chronology on the EW chronology to derive the LW regression residuals that are uncorrelated with EW (i.e., LWa). This manipulation works reasonably well in isolating the variability of LW growth that theoretically should contain a 'discrete' seasonal climate signal that is independent of prior season biological and climate conditions (i.e., Stahle *et al*., 2009; Griffin *et al*., 2011). In this study, the LW width chronology was regressed on the EW width chronology at each site for the common interval from 1838–1991 to produce the LWa width data. The 1838–1991 interval represents the period when most sites contain the highest number of individual samples used in the calculation of the chronologies (i.e., >5 trees sampled).

3.2 | Instrumental climate data and the calculation of onset date of summer rains

Gridded daily precipitation data were acquired from the National Oceanic and Atmospheric Administration (NOAA) Climate Prediction Center's (CPC) U.S. Unified Gauge-Based Analysis of Precipitation dataset (Higgins *et al*., 2000, 2007). The gridded daily data covers the continental United States at 0.25° latitude 0.25° longitude resolution from 1948-present and is updated daily. The daily gridded product is created using a dense network of observing sites from NOAA and the National Climatic Data Center (NCDC) River Forecast Center (RFC) which are then interpolated using an optimal interpolation algorithm that also accounts for complex terrain (Xie *et al*., 2007). The daily totals at each grid point are calculated for the 24-hr period ending at 1200 UTC of the current day. Daily precipitation totals tend to be underestimated in the gridded data when compared to station totals because of spatial interpolation, but when aggregated over longer timescales precipitation totals are similar between gridded products and station data (Ensor and Robeson, 2008). Here, we treat gridded daily precipitation totals <1.00 mm as zero because these values are often an artefact of spatial interpolation and add noise to the common signal that might be present in the tree-ring data (e.g., Howard and Stahle, 2020). Gridded monthly precipitation data from the Global Precipitation Climatology Centre (GPCC; Schneider *et al*., 2018) were used in a 25-year running correlation analysis between July and December–April precipitation from 1891–2016 for a regional average of the southwestern United States (approximately 30°–40°N, 113.5°–103°W) to examine the inter-seasonal relationship between cool season moisture and monsoon rains. The GPCC monthly data were used for the running correlation instead of the daily product simply to extend the analyses prior to 1948.

Calculation of monsoon onset over the NAMS has been analytically derived using a variety of methods based on daily precipitation data and variables that track changes in atmospheric circulation and humidity in early summer (Higgins *et al*., 1997; Ellis *et al*., 2004; Liebmann *et al*., 2008). Here, we use segmented regression to detect changepoints in cumulative daily precipitation time series for the 67 grid points closest to each tree-ring site for the period 1948–1991. With segmented regression, two-segment piecewise linear regression models were fit to each daily precipitation time series using an algorithm in the R package 'Segmented' (Muggeo, 2008). Starting with estimated changepoints for each daily time series based on previous calculations of monsoon onset (e.g., Higgins *et al*., 1997; Ellis *et al*., 2004; Liebmann *et al*., 2008), the algorithm iteratively fits two-segment regression models across a possible range of changepoints and then chooses the model with the lowest residual sum of squares (Muggeo, 2003). The segmented regression approach allows for the manual selection of the start and end dates of the daily time series for which to calculate changepoints. Onset dates were calculated using segmented regression based on daily cumulative time series from Julian day 152 (June 1) to Julian day 243 (August 31). Using different intervals from June 1 to September 30, and June 1 to October 31 did not significantly change the timing of onset dates. This approach is similar to the methods applied by Cook and Buckley (2009), who calculated monsoon onset and withdrawal dates from cumulative daily station data in Thailand using two-phase linear regression. Segmented regression was also applied to calculate summer wet season withdrawal dates for two different intervals (i.e., Julian days 213–273 and 213–303 or August 1–September 30 and August 1–October 31, respectively). However, significantly different withdrawal dates were produced using the two different periods for some grid points, suggesting there is no significant step-like change in cumulative daily precipitation totals that signifies the end of the summer wet season. As a result, instrumental withdrawal dates were not included in this analysis.

3.3 | Calculating the onset, peak correlation, and duration of the LW growth response to precipitation

The daily precipitation data were correlated with the 67 LWa chronologies to investigate four variables associated with the seasonal precipitation signal in the growth of LW. These four variables include the Julian date of onset and withdrawal, peak correlation, and duration (from onset to withdrawal) for the optimal daily

precipitation interval calculated for each LWa chronology. To objectively calculate these variables, daily precipitation data were extracted for the eight grid points closest to each LWa chronology, and then summed for intervals ranging from 10- to 90-days in length ($n = 81$ intervals) from April 1 to September 30 (e.g., a 31-day total for July 31 = precipitation summed from July 1 to July 31 each year, producing an annual time series from 1948–1991 that could then be correlated with the respective LWa chronology). This results in 118,584 annual time series (183 days × 81 intervals × 8 grid points) correlated with each chronology for the common period of 1948–1991. The eight surrounding grid points were all considered instead of the single nearest grid point simply to expand the search radius and to possibly identify nearby grid points where the correlation with precipitation may be higher. Precipitation at a single grid cell tends to have a wider spatial correlation when summed over longer timescales (i.e., 60–90 days). It is therefore possible that higher correlations for longer intervals might be computed for grid points beyond the nearest eight to each chronology, but this was not observed consistently. Inclusion of precipitation totaled for less than 10 days often resulted in annual time series with numerous zero values at drier sites and were excluded. Few if any of the available LWa chronologies are correlated with precipitation summed for more than a 90-day period (Stahle *et al*., 2009; Griffin *et al*., 2011; Griffin, 2013).

The precipitation interval (at any of the eight grid points) from 10- to 90-days with the highest correlation with the nearby LWa chronology was then identified as the 'optimal daily precipitation response interval'. The beginning and ending Julian dates for this optimal interval are the 'onset' and 'withdrawal' dates, respectively, and the 'duration' of the signal is the number of Julian days between onset and withdrawal, similar to the approached defined by Jevšenak (2019). The highest Pearson's correlation coefficient for any interval and day of the year, is referred to as the 'peak correlation'. In these calculations, peak correlation occurs on the withdrawal date and following this day the correlations with precipitation begin to decline. As an example, if the highest single grid point correlation found for a given LWa chronology was with 31-day total precipitation from July 1 to July 31 for 1948–1991 (i.e., the peak correlation), then the onset date would be July 1, withdrawal date would be July 31, and the duration of the signal would be 31 days. The tree-ring chronology will be correlated at a

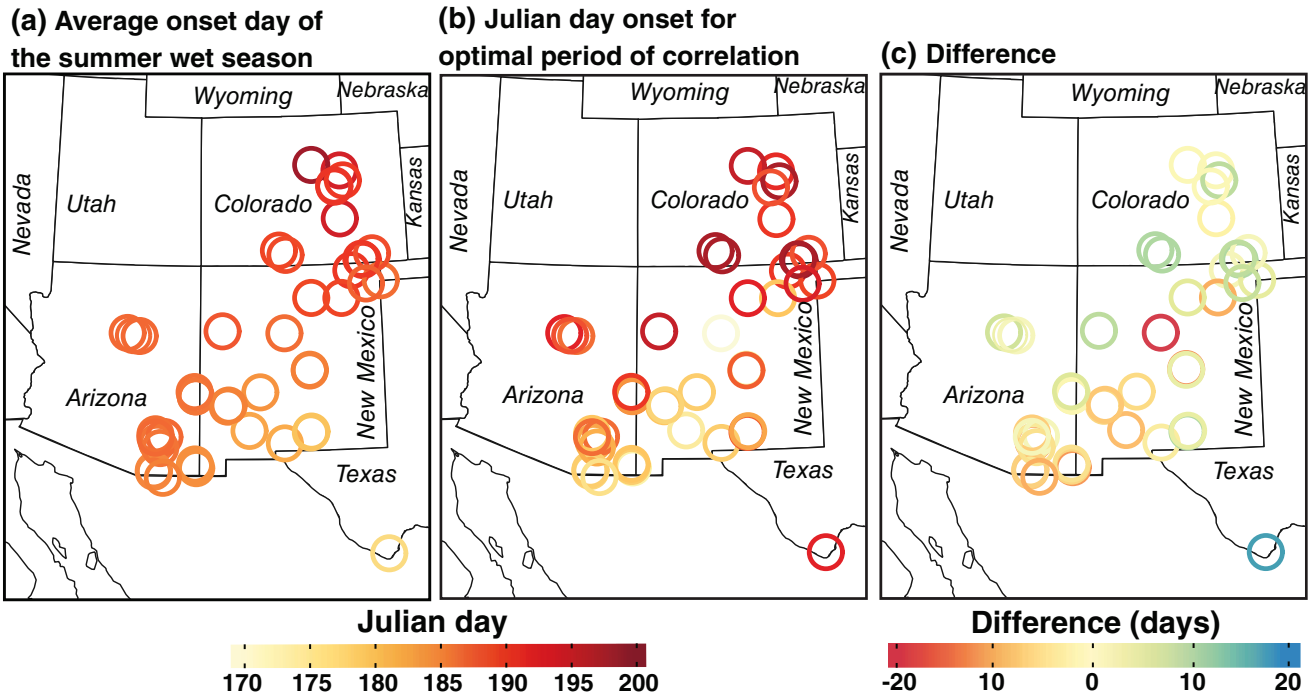

FIGURE 4 (a) The climatological average onset date of the summer wet season was determined for the grid point closest to the 46 LWa chronologies correlated only with summer rainfall using segmented regression models on cumulative daily precipitation data from June 1 to August 31. The average onset date is based on the 1948–1991 period. (b) The tree-ring onset date was determined by identifying the beginning Julian date of the optimal daily precipitation response interval for the 46 LWa chronologies well correlated with summer precipitation. Note the similar latitudinal transitions in onset dates from both the instrumental and tree-ring data (a vs. b). (c) The difference between the instrumental onset dates and tree-ring onset dates (tree ring—instrumental) [Colour figure can be viewed at wileyonlinelibrary.com]

similar but lower level with 31-day precipitation totals before and after the date of the peak correlation simply because the correlations are being advanced just 1 day at a time. But these correlations will always be lower than the peak correlation and the method provides an objective basis for the estimation of onset, duration, and withdrawal of the optimal summer precipitation response.

3.4 | Principal component analysis

Gridded precipitation summed from July 6 to August 3 for a regional average of the southwestern United States (approximately 30°–40°N, 113.5°–103°W) and a network of 46 LWa chronologies that are sensitive only to summer rainfall were both investigated with principal component analyses (PCA; Jolliffe, 2002). The July 6 to August 3 interval represents the average optimal precipitation response period for the 46 LWa chronologies (see Table 1). The PCA based on the LWa chronologies was computed for the full common period from 1838–1991, and for the period from 1948–2019 for the early summer precipitation data. The loadings and first three principal component (PC) time series for both the tree-ring and instrumental data were retained. Loadings on the PCs were mapped to characterize the leading modes of tree growth and early summer precipitation variability over the southwestern United States. The time series from the first two PCs of the LWa chronologies were correlated with PC1 and PC3, respectively, from the early summer instrumental precipitation data over the common period 1948–1991. To investigate the largescale synoptic circulation features associated with these leading modes of tree growth and early summer precipitation variability, the two PC1 time series were correlated with July 500 mb geopotential height and integrated precipitable water and regressed on 850mb vector winds for the period 1948–1991 using data from the NCEP/NCAR Reanalysis 1 dataset (Kalnay *et al*., 1996).

4 | RESULTS

4.1 | The LW growth response to summer precipitation onset and daily totals

The 67 LWa chronologies from the southwestern United States are significantly correlated with local precipitation accumulated over intervals ranging from 10- to 90-days over a six-month warm season extending from April to September. The onset and withdrawal dates, the duration, and the peak correlation computed for the optimal daily precipitation interval for each LWa chronology are listed in Table 1. There are 45 LWa chronologies significantly correlated only with summer moisture, meaning the tree-ring onset date is after Julian day 172 (June 21; Table 1). However, the Sandia LWa chronology is also included as one of the 46 discrete summer moisture proxies even though the onset date for this site is Julian day 167. This LWa chronology was included because of its high correlation with local precipitation from late June through August (Table 1). The remaining 21 chronologies largely have onset dates at least 1 week before the astronomical start of summer on Julian day 172. These LWa chronologies are primarily Douglas-fir sites in western New Mexico and on the Colorado Plateau that are correlated with total precipitation in spring and early summer and thus excluded from the remaining analyses (Table 1). When separated by species, 24 out of the 27 ponderosa

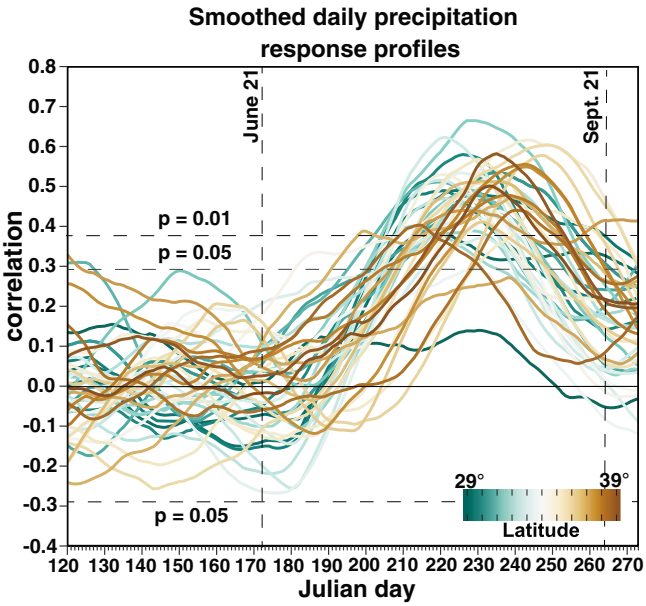

FIGURE 5 The daily precipitation response profiles are plotted for the 46 LWa chronologies best correlated with summer moisture (based on the Pearson's correlation with overlapping 30-day total precipitation intervals, advancing 1 day a time). Each response profile is colour-coded by latitude. The response profiles that peak first tend to be for sites in southern Arizona and New Mexico, while the later peaks are for sites at more northerly latitudes in northern New Mexico and eastern Colorado. All response profiles have been smoothed with a 30-day moving average to reduce the inter-day variability of correlation values and better illustrate differences in timing of peak response based on the location of each chronology. This smoothing procedure delays the timing of the response profiles by an average of 13 days compared to the unsmoothed profiles, but preserves the latitudinal changes among chronologies. The horizontal dashed lines represent significance thresholds (p <.05 and p <.01, two tailed) based on correlations calculated from 1948–1991 (n = 44) [Colour figure can be viewed at wileyonlinelibrary.com]

pine chronologies are significantly correlated with summer precipitation compared to just 22 out of 40 Douglas-fir LWa chronologies (Table 1).

The tree-ring onset dates for the 46 LWa chronologies were compared with the local onset dates of the summer wet season based on the instrumental precipitation data. Instrumental onset dates have a 22-day range from June 25 in west Texas to July 17 over the Front Range of eastern Colorado (Figure 4a). Where the influence of the NAMS is stronger, onset dates of late June are calculated for southern New Mexico, and slightly later in early July over southern Arizona (Figure 4a). Northeastern New Mexico and eastern Colorado are approximately the far northeastern boundary of the NAMS (Douglas *et al.*, 1993), and the onset of the wetter midsummer period begins in mid-July (e.g., Figure 3b,d; Hansen *et al.*, 1978; Howard and Stahle, 2020). There are minor differences when onset dates are calculated for the full instrumental 1948–2019 period instead of 1948–1991, but the period 1948–1991 was used for consistency with the tree-ring data.

The Julian date of tree-ring onset also exhibits a poleward progression from southern Arizona northward into northern New Mexico and eastern Colorado (Figure 4b), in broad agreement with the onset dates of summer precipitation calculated from the instrumental data (Figure 4a). The onset dates for the individual tree-ring chronologies have a 35-day range from June 16 to July 21. The optimal period of correlation with precipitation begins in late June and early July for most LWa chronologies in southern Arizona and New Mexico, but the tree-ring onset dates for sites in north-central Arizona, northern New Mexico and eastern Colorado are approximately 2–3 weeks later in mid-to-late July (Figure 4b). The difference between the instrumental and tree-ring onset dates range from −17 to +18 days across the network, but the majority of the LWa chronologies ($n = 24$) have onset dates that are within 1 week of the instrumental data (Figure 4c). Daily precipitation response profiles using a fixed 30-day duration (rather than identifying the optimal duration) are plotted in Figure 5 and also illustrate the poleward progression of the LW growth response to summer precipitation. These response profiles are based on running correlations with 30-day total precipitation advancing 1 day a time, and then smoothed with a 30-day running mean. The smoothed response profiles show a later Julian date for the peak precipitation correlation as the latitude of the tree-ring chronologies increases poleward (Table 1; Figure 5).

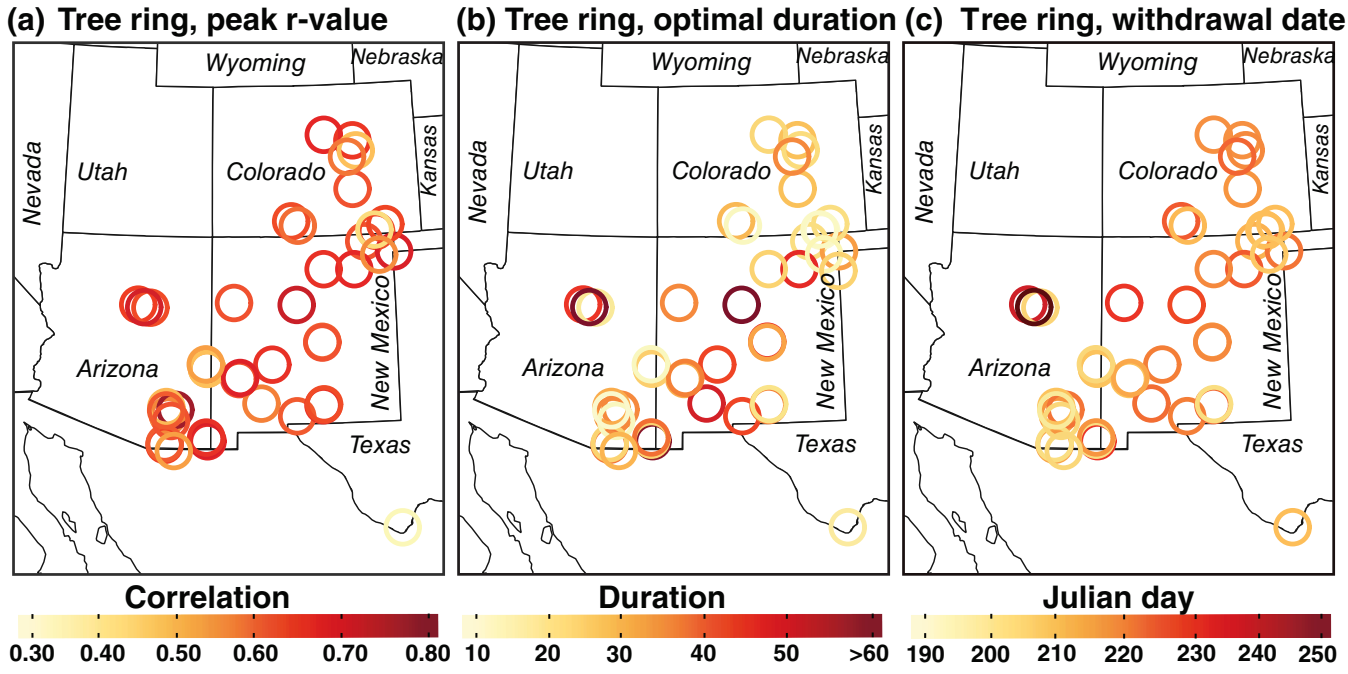

FIGURE 6 (a) The peak Pearson's correlation coefficients for the optimal daily precipitation response intervals are mapped for the 46 LWa chronologies correlated with summer moisture. (b) The duration (in days) of the optimal period of moisture response. (c) The withdrawal dates, or the ending Julian day of the optimal period of moisture response. Note the high correlations between latewood growth and precipitation across the southwestern United States at timescales of approximately 1 month (a) [Colour figure can be viewed at wileyonlinelibrary.com]

4.2 | Peak correlation, duration, and withdrawal

The peak correlations for the 46 LWa chronologies range from 0.39 to 0.81 (mean $r = .62$; Table 1; Figure 6a). When the duration of the optimal daily precipitation intervals is identified for each chronology, values range from 10–62 days with an average of 28.78 days from July 6 to August 3 across the network (Table 1; Figure 6b). Sites with a longer duration (i.e., greater than 45 days) are located primarily in western New Mexico and north-central Arizona. The tree growth response to moisture is largely at sub-monthly timescales in northern New Mexico and Colorado (Figure 6b). Over southeastern Arizona the duration of the optimal response has the highest variability, ranging from 10 to 59 days. The average duration for the Douglas-fir and ponderosa pine LWa chronologies are similar across the southwestern United States, averaging 29.6 and 28.0 days, respectively. The withdrawal date, defined as the ending Julian day of the optimal period of moisture response, resembles the spatial pattern of duration and the earliest dates of withdrawal which occur in late July are estimated for the chronologies in southeastern Arizona (Figure 6b,c).

4.3 | PCA of early summer precipitation and LW width

The first PC calculated for the 46 LWa chronologies from 1838–1991 represents 25.33% of the variance in the correlation matrix and represents a region-wide pattern of similar tree growth anomalies across the southwestern United States (Figure 7a), with the highest loadings in the southern portion of the study area. The loadings on PC1 of the tree-ring chronologies resemble the spatial

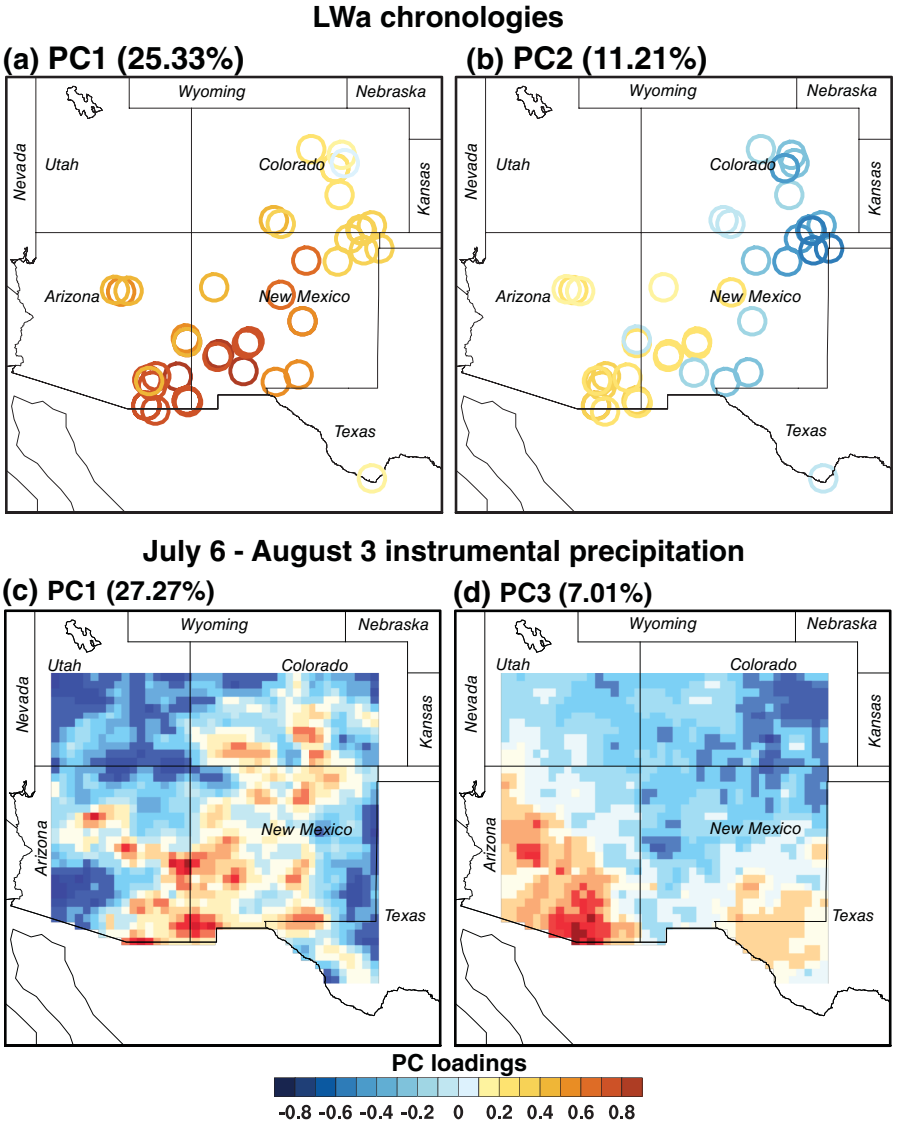

FIGURE 7 A principal component analysis (PCA) was applied to the 46 LWa chronologies for the period 1838–1991. The loadings for the (a) first and (b) second principal components (PCs) are mapped (explained variance listed as %). The loadings from the (c) first and (d) third PCs are mapped based on PCA of gridded July 6 to August 3 precipitation totals for the southwestern United States (approximately 30°–40°N, 113.5°–103°W) from 1948–2019 [Colour figure can be viewed at wileyonlinelibrary.com]

pattern of the first PC of July 6 to August 3 precipitation based on the period 1948–2019, which accounts for 27.27% of the instrumental rainfall variance (Figure 7c). The second most important mode of LWa variability is a spatial pattern that discriminates southern Arizona and New Mexico from northern New Mexico and eastern Colorado (Figure 7b), which is similar to the loadings on PC3 for the instrumental July 6 to August 3 precipitation totals (Figure 7d). When PCA is computed on the instrumental July 6 to August 3 precipitation totals for the common period of 1948–1991, the spatial loading patterns of PC2 and PC3 are similar to the patterns computed for PC1 and PC2 of the tree-ring chronologies. Similar loading patterns are also computed for the tree-ring data when PCA is ran for the period 1948–1991 (not shown). The eigenvector amplitude time series of PC1 from the LWa chronologies is significantly correlated with the PC1 time series of instrumental July 6 to August 3 precipitation ($r = .66$) and reproduces most major wet and dry years of early summer rains over the southwestern United States (Figure 8a). The correlation between the PC2 time series from the tree-ring data and PC3 from July 6 to August 3 precipitation is weaker ($r = .42$; 1948–1991), but the correlation increases to $r = .55$ when the first 10 years of data are omitted (Figure 8b).

The first PCs from the tree-ring and July 6 to August 3 precipitation data were correlated with the 500mb height field and integrated precipitable water and were regressed on 850mb wind vectors for the common period 1948–1991 (Figure 9). Both tree-ring and instrumental PC time series share a negative correlation with the 500mb height field extending from the eastern Pacific into the southern United States with the most significant correlations centred over northwestern Mexico (Figure 9a,b). Regression coefficients of 850mb winds indicate a region of enhanced cyclonic circulation over the southwestern United States and northern Mexico, consistent with southwesterly moisture advection from the Pacific and Gulf of California. Positive correlations with integrated precipitable water are present over much of the interior western United States and northern Mexico and extend westward into the eastern Pacific (Figure 9c,d).

4.4 | Early summer precipitation and LW tree growth correlation with antecedent cool season moisture

The preceding results indicate that LWa chronologies from the southwestern United States are most highly correlated with precipitation during an approximate

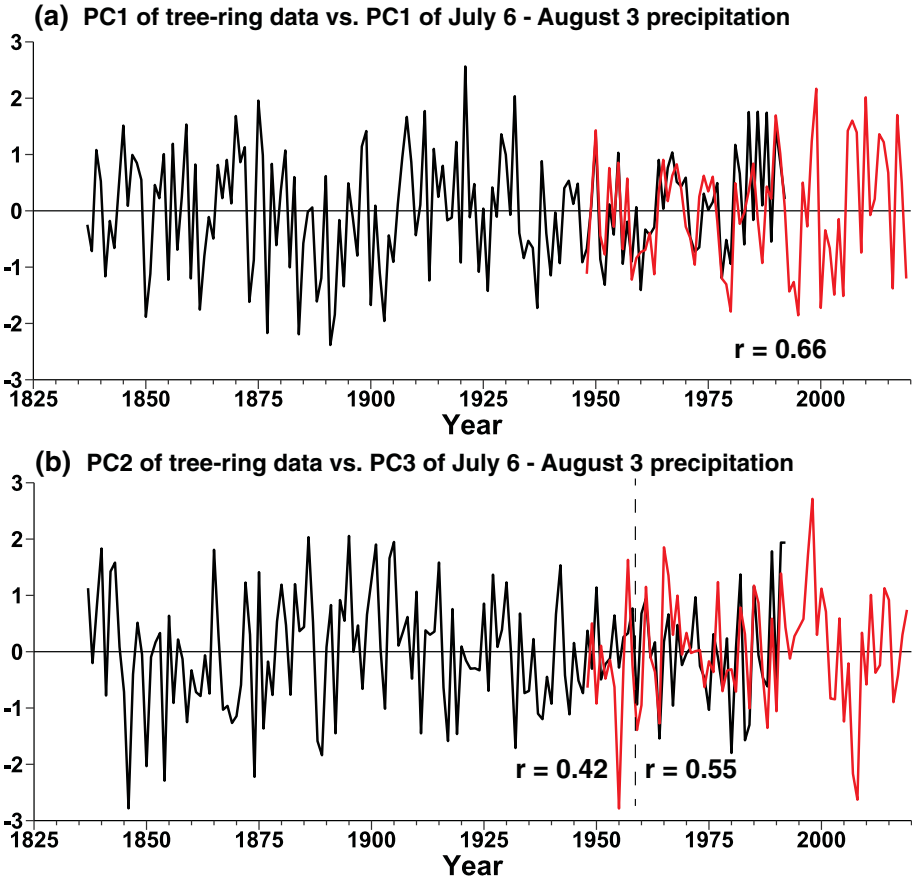

FIGURE 8 (a) The PC1 eigenvector amplitude time series of the LWa chronologies is plotted from 1838–1991 along with the PC1 time series of July 6 to August 3 instrumental precipitation (1948–2019). (b) The time series for the second PC of the tree-ring data and the time series of PC3 of the instrumental data are plotted for the same intervals as in (a). The instrumental and tree-ring time series in (b) are more highly correlated from 1958–1991 ($r = .55$) [Colour figure can be viewed at wileyonlinelibrary.com]

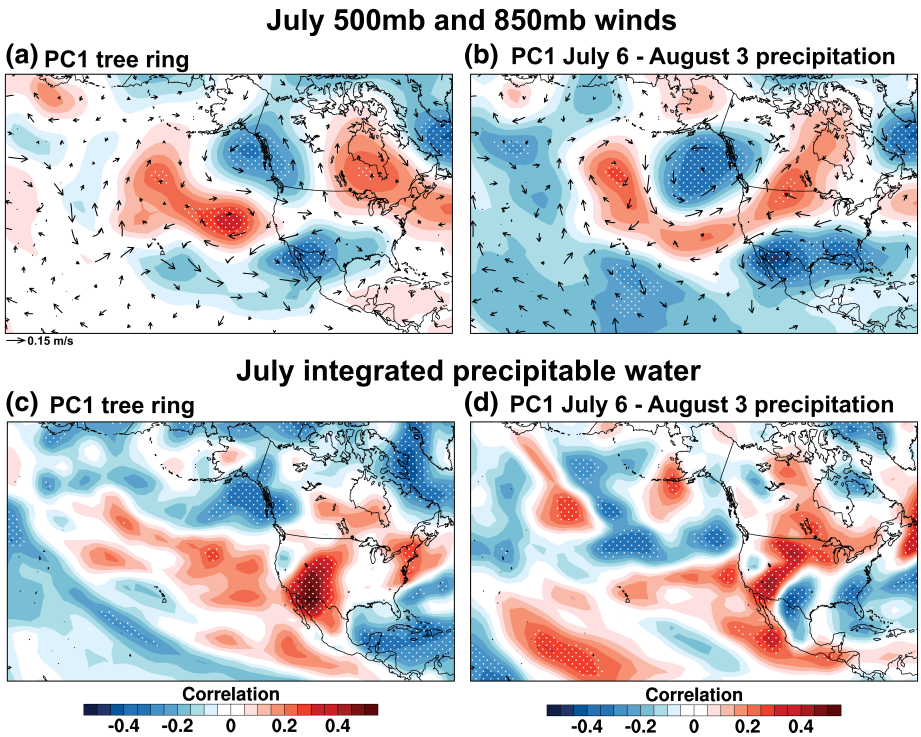

FIGURE 9 (a) The first PC from the LWa chronologies and (b) the first PC from instrumental July 6 to August 3 precipitation for the southwestern United States were correlated with the July 500mb geopotential height and used in a regression with 850mb winds from 1948–1991. Note the negative correlation with 500mb heights and anomalous cyclonic circulation at the lower levels of the atmosphere over northwestern Mexico and the southwestern United States. (c) The first PC from the LWa chronologies and (d) the first PC from instrumental July 6 to August 3 precipitation were correlated with July integrated precipitable water. White stipples indicate areas of significant (p <.05) correlation. Note the positive correlations that extend across much of the eastern Pacific and into western North America. The similar spatial correlation and regression patterns observed for the tree-ring and instrumental PCs suggest that LWa chronologies from the southwestern United States may be useful proxies for the largescale atmospheric circulation anomalies responsible for the leading mode of early summer precipitation variability [Colour figure can be viewed at wileyonlinelibrary.com]

four-week interval in early summer, which for the average of the 46 chronologies extends 29-days from July 6 to August 3. Projections of precipitation during this initial 'month' of the summer wet season indicate slight declines over the coming decades (Cook and Seager, 2013), but the regional average of July 6 to August 3 precipitation totals for the study area does not exhibit significant trend from 1948–2019 (Figure 10a; also, no trend is detected for July precipitation totals from 1891 to 2016). However, above average July 6 to August 3 normalized precipitation was observed in the instrumental data during the 1950s and early 21st century droughts, two of the most severe and sustained cool-season droughts over the area since 1948 (Figure 10a). This includes 1950, 1953, 1955, and 2006–2015 (Figure 10a), and may be relevant to hypothesized dynamics linking cool season moisture and summer rains over the southwestern United States.

Anomalies in the onset and intensity of the summer wet season over the southwestern United States have been linked to snow cover and precipitation during the preceding cool season (Gutzler and Preston, 1997; Gutzler, 2000; Higgins and Shi, 2000; Lo and Clark, 2002), and this weak negative correlation is also detected in comparisons of instrumental and proxy precipitation data for the study area (e.g., Stahle *et al.*, 2009; Griffin *et al.*, 2013). December–April precipitation totals over the study area are anti-correlated with July 6 to August 3 totals in the instrumental data at $r = -.24$ (p <.05) from 1948–2019. This relationship is asymmetric and appears to primarily reflect the tendency for dry conditions in early summer to follow wet extremes in winter and spring (Figure 10a). Student's t-test comparing the 10 wettest December–April totals from 1948–2019 with precipitation during the early summer at each grid point in the study area indicates that the July 6 to August 3 precipitation totals are significantly below average (p <.05) across much of the southwestern United States following wet winters (Figure 10b). However, the 10 driest December–April totals do not coincide with unusually wet conditions in early summer (Figure 10c).

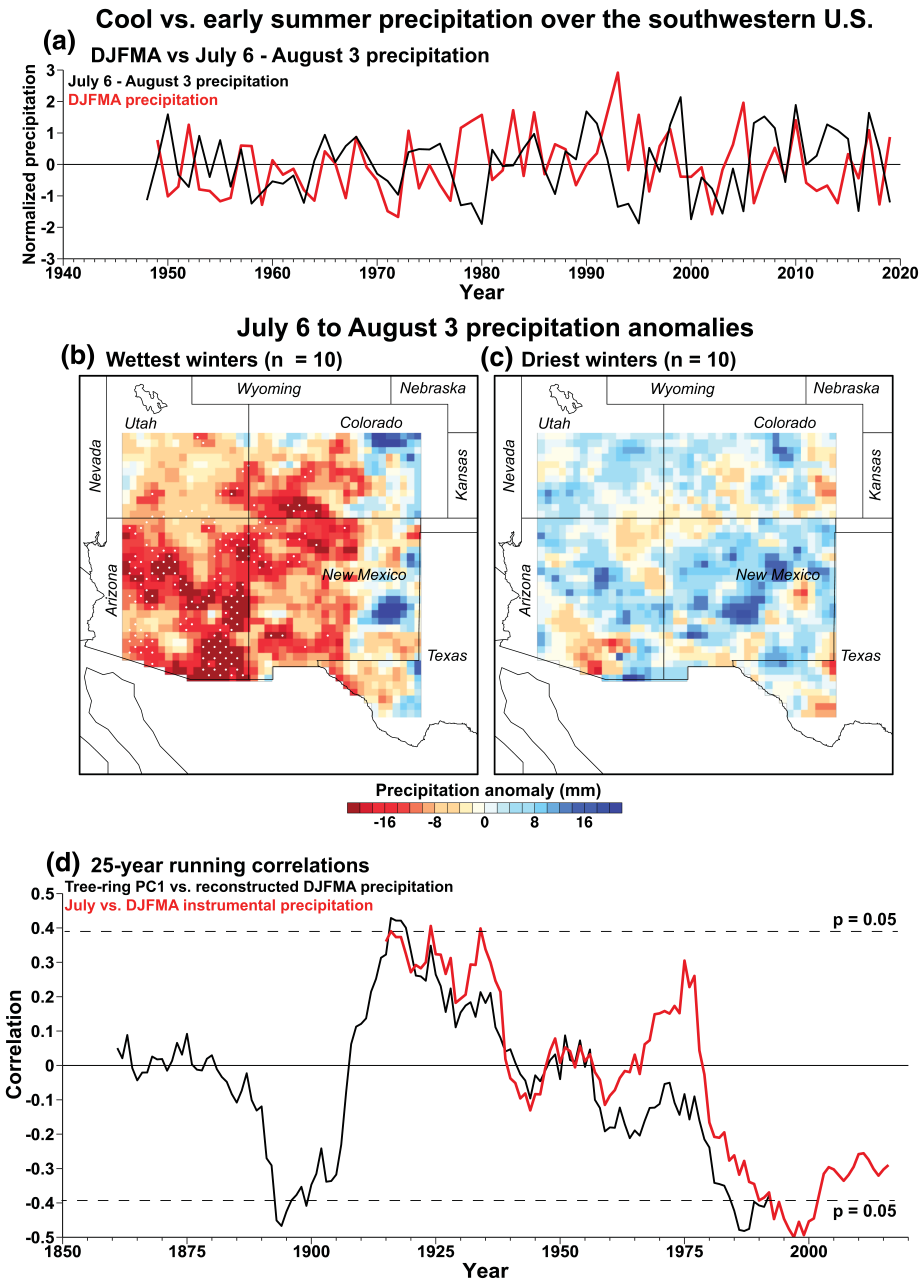

FIGURE 10 (a) A time series comparison between normalized December–April (DJFMA) and July 6 to August 3 precipitation totals from 1948–2019 ($r = -.24$; $p < .05$). Note the stronger anti-phasing between seasons following wet winters over much of the southwestern United States. (d) Regional average instrumental December–April and July precipitation totals were used in 25-year running correlation analyses from 1891 to 2016 to examine the relationship between early summer rains and antecedent cool season moisture. A 25-year running correlation analysis was also used to examine the relationship between the first PC from the LWa chronologies and a regional average of December–April precipitation reconstructions from the North American Seasonal Precipitation Atlas (Stahle *et al.*, 2020). Dashed lines indicate $p < .05$ significance. Note the similarities in running correlations between the instrumental and tree-ring reconstructed data, which exhibit strong multi-decadal variability and episodes of both significant positive and negative correlations [Colour figure can be viewed at wileyonlinelibrary.com]

Twenty-five year running correlations from 1891–2016 between instrumental December–April and July precipitation indicate that the anti-correlation is mainly present in the latter half of the instrumental record, and in fact there were short episodes of significant positive correlation during the early 20th century (Figure 10d). The PC1 time series of LWa, a proxy for early summer season precipitation (July 6 to August 3), was also correlated with a regional average of tree-ring reconstructed December–April total precipitation from the North American Seasonal Precipitation Atlas (NASPA; Stahle *et al.*, 2020). The regional average of the cool season reconstructions is not correlated with PC1 over the full common period from 1838–1991, but there are multi-decadal episodes of significant positive and negative correlations based on 25-year running correlations. The correlation with the cool season reconstruction is as low as $r = -.49$ from 1963 to 1987 and as high as $r = +0.42$ from 1892–1916. The significant negative correlation from 1871–1895 ($r = -.44$; Figure 10d) based on the tree-ring data is primarily the result of above-normal reconstructed cool season precipitation coinciding with negative PC1 values (not shown), which is similar to the asymmetry identified between instrumental cool season and July 6 to August 3 precipitation totals from 1948–2019 (Figures 10a–c).

The low-frequency changes in inter-seasonal correlation computed for the tree-ring data are similar to the changes computed for the instrumental data during the

20th century (Figure 10d). These results suggest that the weak relationship between early summer precipitation and antecedent cool season moisture has been both asymmetrical and subject to multi-decadal changes. If real, this asymmetry and multi-decadal variability might provide some insight into the onset and intensity of early summer moisture over the southwestern United States.

5 | DISCUSSION AND CONCLUSIONS

In this study, we used instrumental daily precipitation data to identify the Julian date of summer precipitation onset for locations across the southwestern United States. A network of tree-ring chronologies was then used to determine the optimal timing and duration of the LW width response to summer precipitation. Based on segmented regression analyses of instrumental daily precipitation, the average onset date of the local summer wet season becomes progressively later in summer from south to north across the southwestern United States, with the earliest onset dates in late June over far west Texas and southern New Mexico. Further northward in eastern Colorado, average onset dates are approximately 2–3 weeks later in mid-July. This poleward lag in onset dates is in line with previous studies of monsoon onset over North America (Higgins *et al*., 1997; Ellis *et al*., 2004; Liebmann *et al*., 2008). The average Julian day onset of the optimal correlation between the 46 LWa chronologies and summer precipitation parallels the poleward progression of onset measured in the instrumental data. This suggests an important bioclimatic coupling between LW formation and the local climatology of early summer rains. It might therefore be possible to use this tree growth and climate coupling to reconstruct the local onset of early summer precipitation across the NAMS region using the extensive network of LW width chronologies from Mexico (Villanueva-Díaz *et al*., 2017) and the southwestern United States.

The LWa chronologies respond to the amount of early summer precipitation across the southwestern United States. The strongest summer precipitation correlations with LWa width are calculated for an average of approximately 1-month during early summer following the onset of the local summer wet season (mean = 28.78 days from July 6 to August 3). These optimal correlations with early summer precipitation totals range from just 10 to 62 days for the subset of 46 summer sensitive LWa chronologies of Douglas-fir and ponderosa pine, with the correlations ranging from 0.39 to 0.81 (mean r = .62). The shortest intervals of daily precipitation response after onset were generally detected in Douglas-fir (i.e., 14 of the 21 chronologies with an optimal duration less than 20 days were Douglas-fir; Table 1). Douglas-fir LWa chronologies from southern Arizona have some of the highest correlations with summer moisture in the entire network, but Douglas-fir chronologies from the Colorado Plateau region are often not well correlated with summer precipitation. Instead, Colorado Plateau Douglas-fir tend to be best correlated precipitation prior to the local onset of the monsoon season. Griffin *et al*. (2013) found similar results based on PCA of LW width chronologies from the southwestern United States.

The 46 summer sensitive LWa chronologies analysed in this study reproduce the leading mode of early summer precipitation variability documented in the instrumental observations over the southwestern United States, which is a region wide pattern of precipitation and tree growth covariability that extends from southeastern Arizona northeastward to eastern Colorado (Figure 7a). The leading modes of tree growth and early summer precipitation variability are both negatively correlated with 500mb heights over the southwestern United States and northern Mexico, indicating that a mid-level trough was often present during years of abundant early summer moisture and positive tree growth anomalies. A trough at the 500mb level would favour enhanced counterclockwise air flow at 850mb leading to advection of atmospheric moisture from the Gulf of California that also results in an increase in precipitable water over northern Mexico and the study region. These atmospheric circulation observations for above average precipitation and abundant LW growth conditions in July are consistent with the findings of Higgins *et al*. (1997) for the full monsoon season (June–September). The PC1 time series of LWa growth may therefore represent a useful proxy for reconstructing region-wide wet and dry anomalies and the major synoptic controls on these regimes during the initiation phase of the NAMS over the southwestern United States.

Western North American cool season precipitation and snow cover may play a role in monsoon extent and intensity through land-surface feedbacks and ocean-atmospheric teleconnections (Gutzler, 2000; Ellis and Hawkins, 2001; Lo and Clark, 2002), which could have skill in forecasting summer monsoon rains (Hawkins and Ellis, 2002). Our preliminary results based on tree-ring and instrumental precipitation data indicate that early summer rains and LW tree growth are both modestly but negatively correlated with cool season precipitation since the mid-20th century, similar to the findings of Griffin *et al*. (2013). Episodes of anti-correlation in the modern and pre-instrumental records tend to be asymmetric and largely driven by wet cool seasons that are followed by dry early summers. Above-normal precipitation and

snow cover in winter and spring may have a greater impact on summer monsoon rains because abundant soil moisture can weaken the land-ocean thermal gradient necessary for strong monsoon circulation (Lo and Clark, 2002). However, the negative correlation between cool and early warm season precipitation is subject to major changes on multidecadal time scales in both the instrumental record, and in comparisons between tree-ring reconstructed cool season precipitation and LW growth since the early 19th century (see also Griffin *et al*., 2013). In fact, decadal episodes of significant positive correlations are identified in the tree-ring data (Figure 10d).

Gutzler (2000) noted that the relationship between spring snowpack and monsoon rains has been unstable in the modern era and possibly modulated by different combinations of tropical and extratropical Pacific sea-surface temperature (SST) patterns and atmospheric circulation anomalies over the North Pacific (Higgins and Shi, 2000; Mo and Paegle, 2000). Mo and Paegle (2000) found that years of anti-phasing between winter precipitation and monsoon rains over the southwestern United States are linked with a mode of seasonal SST variability that includes El Niño-like conditions in the tropical Pacific during the cool season and positive SST anomalies over the eastern Pacific in summer. This mode of seasonal SST variability promotes wetter conditions during winter, but summers tend to be drier because the southwestern United States is located under a descending branch of the Hadley Circulation (Higgins *et al*., 1998; Mo and Paegle, 2000).

Contrary to the anti-phasing, there have been a number of examples when wet cool season conditions persisted into early summer, and even more cases of a dry cool season followed by a dry early summer, especially prior to 1948. Some years of seasonal persistence are linked with a mode of North Pacific SST variability that tends to persist from winter to summer, but this mode is also subject to strong decadal variability in the instrumental record (Mo and Paegle, 2000). This multidecadal variability of interseasonal correlation may therefore arise from both stochastic and identifiable ocean-atmospheric processes. The long-term variability of cool and early summer precipitation over the southwestern United States can now be investigated for the past several centuries using gridded reconstructions of winter–spring precipitation (e.g., Stahle *et al*., 2020) and LWa proxies of early summer moisture. Extension of these analyses into Mexico could provide a long-term perspective on the inter-annual to decadal variability of the NAMS and its relationship to antecedent cool season conditions and large-scale climate dynamics (e.g., Higgins *et al*., 1997; Stahle *et al*., 2016).

ACKNOWLEDGEMENTS

The National Science Foundation funded this study (grant numbers AGS-1266014 and AGS-1702894). The authors thank Peter Brown, David Meko, and Connie Woodhouse for access to their collections, and Song Feng for providing helpful discussions. The authors are also grateful to Professor Hans Linderholm and a reviewer whose comments improved the manuscript.

ORCID

Ian M. Howard https://orcid.org/0000-0002-8361-9575

REFERENCES

Adams, D.K. and Comrie, A.C. (1997) The North American monsoon. *Bulletin of the American Meteorological Society*, 78(10), 2197:221a3. https://doi.org/10.1175/1520-0477(1997)078<2197:TNAM>2.0.CO;2.

Anchukaitis, K.J., Evans, M.N., Kaplan, A., Vaganov, E.A., Hughers, M.K., Grissino-Mayer, H.D. and Cane, M.A. (2006) Forward modeling of regional scale tree-ring patterns in the southeastern United States and the recent influence of summer drought. *Geophysical Research Letters*, 33(4), L04705. https://doi.org/10.1029/2005gl025050.

Beck, W., Sanders, T.G.M. and Pofahl, U. (2013) CLIMTREG: detecting temporal changes in climate-growth reactions - a computer program using intra-annual daily and yearly moving time intervals of variable width. *Dendrochronologia*, 31(3), 232–241. https://doi.org/10.1016/j.dendro.2013.02.003.

Cleaveland, M.K. (1986) Climatic response of densitometric properties in semiarid site tree rings. *Tree-Ring Bulletin*, 46, 13–29.

Cleaveland, M.K., Stahle, D.W., Therrell, M.D., Villanueva-Diaz, J. and Burns, B.T. (2003) Tree-ring reconstructed winter precipitation and tropical teleconnections in Durango, Mexico. *Climatic Change*, 59(3), 369–388. https://doi.org/10.1023/A:1024835630188.

Cook, B.I. and Buckley, B.M. (2009) Objective determination of monsoon season onset, withdrawal, and length. *Journal of Geophysical Research Atmospheres*, 114(D23), D23109. https://doi.org/10.1029/2009jd012795.

Cook, B.I. and Seager, R. (2013) The response of the north American monsoon to increased greenhouse gas forcing. *Journal of Geophysical Research Atmospheres*, 118(4), 1690–1699. https://doi.org/10.1002/jgrd.50111.

Cook E.R. (1985) *A time series analysis approach to tree ring standardization*. PhD Thesis, University of Arizona.

Crawford, C.J., Griffin, D. and Kipfmueller, K.F. (2015) Capturing season-specific precipitation signals in the northern Rocky Mountains, USA, using earlywood and latewood tree rings. *Journal of Geophysical Research: Biogeosciences*, 120(3), 428–440. https://doi.org/10.1002/2014jg002740.

Dannenberg, M.P. and Wise, E.K. (2016) Seasonal climate signals from multiple tree ring metrics: a case study of *Pinus ponderosa* in the upper Columbia River basin. *Journal of Geophysical Research: Biogeosciences*, 121(4), 1178–1189. https://doi.org/10.1002/2015jg003155.

Deslauriers, A., Morin, H., Urbinati, C. and Carrer, M. (2003) Daily weather response of balsam fir (*Abies balsamea* [L.] mill.) stem radius increment from dendrometer analysis in the boreal

forests of Québec (Canada). *Trees - Structure and Function*, 17, 477–448. https://doi.org/10.1007/s00468-003-0260-4.

Douglas, M.W., Maddox, R.A., Howard, K. and Reyes, S. (1993) The Mexican monsoon. *Journal of Climate*, 6(8), 1665–1677. https://doi.org/10.1175/1520-0442(1993)006<1665:TMM>2.0.CO;2.

Douglass, A.E. (1920) Evidence of climatic effects in the annual rings of trees. *Ecology*, 1(1), 24–32. https://doi.org/10.2307/1929253.

Ellis, A.W. and Hawkins, T.W. (2001) An apparent atmospheric teleconnection between snow cover and the north American monsoon. *Geophysical Research Letters*, 28(13), 2653–2656. https://doi.org/10.1029/2000gl006125.

Ellis, A.W., Saffell, E.M. and Hawkins, T.W. (2004) A method for defining monsoon onset and demise in the southwestern USA. *International Journal of Climatology*, 24(2), 247–265. https://doi.org/10.1002/joc.996.

Ensor, L.A. and Robeson, S.M. (2008) Statistical characteristics of daily precipitation: comparisons of gridded and point datasets. *Journal of Applied Meteorology and Climatology*, 47(9), 2468–2476. https://doi.org/10.1175/2008JAMC1757.1.

Faulstich, H.L., Woodhouse, C.A. and Griffin, D. (2013) Reconstructed cool- and warm-season precipitation over the tribal lands of northeastern Arizona. *Climatic Change*, 118, 457–468. https://doi.org/10.1007/s10584-012-0626-y.

Fritts, H.C. (1976) *Tree Rings and Climate*. New York: Academic Press.

Germaine, H.L. and McPherson, G.R. (1998) Effects of timing of precipitation and acorn harvest date on emergence of *Quercus emoryi*. *Journal of Vegetation Science*, 9(2), 157–160. https://doi.org/10.2307/3237114.

Grantz, K., Rajagopalan, B., Clark, M., and Zagona, E. (2007) Seasonal shifts in the north american monsoon. *Journal of Climate*, 20(9), 1923–1935. https://doi.org/10.1175/jcli4091.1.

Griffin, D. (2013). *North American Monsoon Paleoclimatology from Tree Rings*. PhD Thesis, University of Arizona.

Griffin, D., Meko, D.M., Touchan, R., Leavitt, S.W. and Woodhouse, C.A. (2011) Latewood chronology development for summer-moisture reconstruction in the US southwest. *Tree-Ring Research*, 67(2), 87–101. https://doi.org/10.3959/2011-4.1.

Griffin, D., Woodhouse, C.A., Meko, D.M., Stahle, D.W., Faulstich, H.L., Carrillo, C.A., Touchan, R., Castro, C.L. and Leavitt, S.W. (2013) North American monsoon precipitation reconstructed from tree-ring latewood. *Geophysical Research Letters*, 40(5), 954–958. https://doi.org/10.1002/grl.50184.

Gutzler, D.S. (2000) Covariability of spring snowpack and summer rainfall across the Southwest United States. *Journal of Climate*, 13(22), 4018–4027. https://doi.org/10.1175/1520-0442(2000)013<4018:COSSAS>2.0.CO;2.

Gutzler, D.S. and Preston, J.W. (1997) Evidence for a relationship between spring snow cover in North America and summer rainfall in New Mexico. *Geophysical Research Letters*, 24(17), 2207–2210. https://doi.org/10.1029/97GL02099.

Hales, J.E. (1972) Surges of maritime tropical air northward over the Gulf of California. *Monthly Weather Review*, 100(4), 298–306. https://doi.org/10.1175/1520-0493(1972)100<0298:somtan>2.3.co;2.

Hansen, W.R., Chronic, J. and Matelock, J. (1978) Climatography of the front range urban corridor and vicinity, Colorado. *Arctic and Alpine Research*, 10, 786. https://doi.org/10.2307/1550746.

Hawkins, T.W. and Ellis, A.W. (2002) Intra-annual analysis of the north American snow cover-monsoon teleconnection: seasonal forecasting utility. *Journal of Climate*, 15(13), 1743–1753. https://doi.org/10.1175/1520-0442(2002)015<1743:iaaotn>2.0.co;2.

Higgins, R.W., Mo, K.C. and Yao, Y. (1998) Interannual variability of the U.S. summer precipitation regime with emphasis on the southwestern monsoon. *Journal of Climate*, 11(10), 2582–2606. https://doi.org/10.1175/1520-0442(1998)011<2582:IVOTUS>2.0.CO;2.

Higgins, R.W. and Shi, W. (2000) Dominant factors responsible for interannual variability of the summer monsoon in the southwestern United States. *Journal of Climate*, 13(4), 759–776. https://doi.org/10.1175/1520-0442(2000)013<0759:dfrfiv>2.0.co;2.

Higgins, R.W., Shi, W., Yarosh, E., and Joyce, R. (2000) *Improved United States Precipitation Quality Control System and Analysis*. In NOAA, National Weather Service, National Centers for Environmental Prediction, Climate Prediction Center.

Higgins, R.W., Silva, V.B.S., Shi, W. and Larson, J. (2007) Relationships between climate variability and fluctuations in daily precipitation over the United States. *Journal of Climate*, 20(14), 3561–3579. https://doi.org/10.1175/JCLI4196.

Higgins, R.W., Yao, Y. and Wang, X.L. (1997) Influence of the north American monsoon system on the US. summer precipitation regime. *Journal of Climate*, 10(10), 2600–2622. https://doi.org/10.1175/1520-0442(1997)010<2600:iotnam>2.0.co;2.

Howard, I.M., Stahle, D.W. and Feng, S. (2019) Separate tree-ring reconstructions of spring and summer moisture in the northern and southern Great Plains. *Climate Dynamics*, 52, 5877–5897. https://doi.org/10.1007/s00382-018-4485-8.

Howard, I.M. and Stahle, D.W. (2020) Tree-ring reconstruction of single-day precipitation totals over eastern Colorado. *Monthly Weather Review*, 148(2), 597–612. https://doi.org/10.1175/MWR-D-19-0114.1.

Jevšenak, J. (2019) Daily climate data reveal stronger climate-growth relationships for an extended European tree-ring network. *Quaternary Science Reviews*, 221, 105868. https://doi.org/10.1016/j.quascirev.2019.105868.

Jolliffe, I.T. (2002) *Principal Component Analysis*. New York: Springer.

Kalnay, E., Kanamitsu, M., Kistler, R., Collins, W., Deaven, D., Gandin, L., Iredell, M., Saha, S., White, G., Woollen, J., Zhu, Y., Chelliah, M., Ebisuzaki, W., Higgins, R.W., Janowiak, J., Mo, K.C., Ropelewski, C., Wang, J., Leetmaa, A., Reynolds, R., Jenne, R. and Joseph, D. (1996) The NCEP/NCAR 40-year reanalysis project. *Bulletin of the American Meteorological Society*, 77(3), 437–472. https://doi.org/10.1175/1520-0477(1996)077<0437:tnyrp>2.0.co;2.

Land, A., Remmele, S., Schönbein, J., Küppers, M. and Zimmermann, R. (2017) Climate-growth analysis using long-term daily-resolved station records with focus on the effect of heavy precipitation events. *Dendrochronologia*, 45, 156–164. https://doi.org/10.1016/j.dendro.2017.08.005.

Lebourgeois, F., Bréda, N., Ulrich, E. and Granier, A. (2005) Climate-tree-growth relationships of European beech (*Fagus sylvatica* L.) in the French permanent plot network (RENECOFOR). *Trees - Structure and Function*, 19, 385–401. https://doi.org/10.1007/s00468-004-0397-9.

Liebmann, B., Bladé, I., Bond, N.A., Gochis, D., Allured, D. and Bates, G.T. (2008) Characteristics of north American summertime rainfall with emphasis on the monsoon. *Journal of Climate*, 21(6), 1277–1294. https://doi.org/10.1175/2007JCLI1762.1.

Lo, F. and Clark, M.P. (2002) Relationship between spring snow mass and summer precipitation in the southwestern United States associated with the north American monsoon system. *Journal of Climate*, 15(11), 1378–1385. https://doi.org/10.1175/1520-0442(2002)015<1378:RBSSMA>2.0.CO;2.

McDowell, N.G., Williams, A.P., Xu, C., Pockman, W.T., Dickman, L.T., Sevanto, S., Pangle, R., Limousin, J., Plaut, J., Mackay, D.S., Ogee, J., Domec, J.C., Allen, C.D., Fisher, R.A., Jiang, X., Muss, J.D., Breshears, D.D., Rauscher, S.A. and Koven, C. (2016) Multi-scale predictions of massive conifer mortality due to chronic temperature rise. *Nature Climate Change*, 6, 295–300. https://doi.org/10.1038/nclimate2873.

Meko, D. (1981). *Applications of Box-Jenkins methods of time series analysis to the reconstruction of drought from tree rings*. PhD Thesis, The University of Arizona.

Meko, D.M. and Baisan, C.H. (2001) Pilot study of latewood-width of conifers as an indicator of variability of summer rainfall in the north American monsoon region. *International Journal of Climatology*, 21(6), 697–708. https://doi.org/10.1002/joc.646.

Mo, K.C. and Paegle, J.N. (2000) Influence of sea surface temperature anomalies on the precipitation regimes over the Southwest United States. *Journal of Climate*, 13(20), 3588–3598. https://doi.org/10.1175/1520-0442(2000)013<3588:IOSSTA>2.0.CO;2.

Muggeo, V. (2003) Estimating regression models with unknown break-points. *Statistics in Medicine*, 22(19), 3055–3071. https://doi.org/10.1002/sim.1545.

Muggeo, V. (2008) Segmented: an R package to fit regression models with broken-line relationships R News. *R News*, 8(1), 20–25. http://cran.r-project.org/doc/Rnews/Rnews_2008-1.pdf.

Ray, A.J., Garfin, G.M., Wilder, M., Vásquez-León, M., Lenart, M. and Comrie, A.C. (2007) Applications of monsoon research: opportunities to inform decision making and reduce regional vulnerability. *Journal of Climate*, 20(9), 1608–1627. https://doi.org/10.1175/JCLI4098.1.

Reiter, E.R. and Tang, M. (1984) Plateau effects on diurnal circulation patterns. *Monthly Weather Review*, 112(4), 638–651. https://doi.org/10.1175/1520-0493(1984)112<0638:peodcp>2.0.co;2.

Schneider, U., Becker, A., Finger, P., Meyer-Christoffer, A., Rudolf, B. and Ziese, M. (2018) *GPCC Full Data Monthly Product Version 2018 at 1.0°: Monthly Land-Surface Precipitation from Rain-Gauges built on GTS-based and Historical Data*. Germany: GPCC. https://doi.org/10.5676/dwd_gpcc/fd_m_v2018_100.

Stahle, D.W., Cleaveland, M.K., Grissino-Mayer, H.D., Griffin, R.D., Fye, F.K., Therrell, M.D., Burnette, D.J., Meko, D.M. and Villanueva Diaz, J. (2009) Cool-and warm-season precipitation reconstructions over western New Mexico. *Journal of Climate*, 22(13), 3729–3750. https://doi.org/10.1175/2008JCLI2752.1

Stahle, D.W., Cook, E.R., Burnette, D.J., Torbenson, M.C.A., Howard, I.M., Griffin, D., Diaz, J.V., Cook, B.I., Williams, A.P., Watson, E., Sauchyn, D.J., Pederson, N., Woodhouse, C.A., Pederson, G.T., Meko, D., Coulthard, B. and Crawford, C.J. (2020) Dynamics, variability, and change in seasonal precipitation reconstructions for North America. *Journal of Climate*, 33 (8), 3173–3195. https://doi.org/10.1175/jcli-d-19-0270.1.

Stahle, D.W., Cook, E.R., Burnette, D.J., Villanueva, J., Cerano, J., Burns, J.N., Griffin, D., Cook, B.I., Acuña, R., Torbenson, M.C. A., Sjezner, P. and Howard, I.M. (2016) The Mexican drought atlas: tree-ring reconstructions of the soil moisture balance during the late pre-Hispanic, colonial, and modern eras. *Quaternary Science Reviews*, 149(1), 34–60. https://doi.org/10.1016/j.quascirev.2016.06.018.

Swetnam, T.W. and Betancourt, J.L. (1998) Mesoscale disturbance and ecological response to decadal climatic variability in the American southwest. *Journal of Climate*, 11(12), 3128–3147. https://doi.org/10.1175/1520-0442(1998)011<3128:mdaert>2.0.co;2.

Szejner, P., Wright, W.E., Babst, F., Belmecheri, S., Trouet, V., Leavitt, S.W., Ehleringer, J.R. and Monson, R.K. (2016) Latitudinal gradients in tree ring stable carbon and oxygen isotopes reveal differential climate influences of the North American Monsoon System. *Journal of Geophysical Research: Biogeosciences*, 121(7), 1978–1991. https://doi.org/10.1002/2016JG003460.

Szejner, P., Wright, W.E., Belmecheri, S., Meko, D., Leavitt, S.W., Ehleringer, J.R. and Monson, R.K. (2018) Disentangling seasonal and interannual legacies from inferred patterns of forest water and carbon cycling using tree-ring stable isotopes. *Global Change Biology*, 24(11), 5332–5347. https://doi.org/10.1111/gcb.14395.

Tang, M. and Reiter, E.R. (1984) Plateau monsoons of the northern hemisphere: a comparison between North America and Tibet. *Monthly Weather Review*, 112(4), 617–637. https://doi.org/10.1175/1520-0493(1984)112<0617:pmotnh>2.0.co;2.

Therrell, M.D., Stahle, D.W., Cleaveland, M.K. and Villanueva-Diaz, J. (2002) Warm season tree growth and precipitation over Mexico. *Journal of Geophysical Research Atmospheres*, 107 (D14), ACL 6-1–ACL 6-8. https://doi.org/10.1029/2001JD000851.

Torbenson, M.C.A. and Stahle, D.W. (2018) The relationship between cool and warm season moisture over the Central United States, 1685-2015. *Journal of Climate*, 31(19), 7909–7924. https://doi.org/10.1175/JCLI-D-17-0593.1.

Torbenson, M.C.A., Stahle, D.W., Villanueva Díaz, J., Cook, E.R. and Griffin, D. (2016) The relationship between Earlywood and latewood ring-growth across North America. *Tree-Ring Research*, 72 (2), 53–66. https://doi.org/10.3959/1536-1098-72.02.53.

Villanueva-Díaz, J., Estrada, J., and Matine, A.R. (2017) El Monzón de Norte América y su influencia en la variabilidad hidro climática de la cuenca alta del Río Nazas. INIFAP, Folleto Técnico Num. 42. ISBN: 978-607-37-0836-4.

Villanueva-Diaz, J., Stahle, D.W., Luckman, B.H., Cerano-Paredes, J., Therrell, M.D., Cleaveland, M.K., and Cornejo-Oviedo, E. (2007) Winter-spring precipitation reconstructions from tree rings for northeast Mexico. *Climatic Change*, 83(1-2), 117–131. https://doi.org/10.1007/s10584-006-9144-0.

Watson, E. and Luckman, B.H. (2002) The dendroclimatic signal in Douglas-fir and ponderosa pine tree-ring chronologies from the southern Canadian cordillera. *Canadian Journal of Forest Research*, 32(10), 1858–1874. https://doi.org/10.1139/x02-096.

Williams, A.P., Allen, C.D., Macalady, A.K., Griffin, D., Woodhouse, C.A., Meko, D.M., Swetnam, T.W., Rauscher, S.A., Seager, R., Grissino-Mayer, H.D., Dean, J.S., Cook, E.R., Gangodagamage, C., Cai, M. and Mcdowell, N.G. (2013) Temperature as a potent driver of regional forest drought stress and tree mortality. *Nature Climate Change*, 3, 292–297. https://doi.org/10.1038/nclimate1693.

Woodhouse, C.A. and Brown, P.M. (2001) Tree-ring evidence for Great Plains drought. *Tree-Ring Research*, 57(1), 89–103.

Woodhouse, C.A., Meko, D.M., Griffin, D. and Castro, C.L. (2013) Tree rings and multiseason drought variability in the lower Rio Grande Basin, USA. *Water Resources Research*, 49(2), 844–850. https://doi.org/10.1002/wrcr.20098.

Xie, P., Yatagai, A., Chen, M., Hayasaka, T., Fukushima, Y., Liu, C. and Yang, S. (2007) A gauge-based analysis of daily precipitation over East Asia. *Journal of Hydrometeorology*, 8(3), 607–626. https://doi.org/10.1175/JHM583.1.

How to cite this article: Howard IM, Stahle DW, Torbenson MCA, Griffin D. The summer precipitation response of latewood tree-ring chronologies in the southwestern United States. *Int J Climatol*. 2021;41:2913–2933. https://doi.org/10.1002/joc.6997